

Packaging of Surface Micromachined Thin Film Thermocouples (TFT): Comparison of the Resistance Arc Microwelding Technique With Wire Bonding

Nipun Sinha, Hee Seok Ahn, Randall Williams, and Debjyoti Banerjee

Abstract—In this paper, we report the packaging of thin film thermocouples (TFT) using resistance arc welding technique. Parallel gap welding and spot welding have been reported in the literature for attaching thin wires to metal thin films. To the knowledge of the authors, this is the first time resistance arc welding has been reported as a packaging technique for microfabricated devices. A brief description of the microfabrication process and chemical analysis using X-ray photoelectron spectroscopy (XPS) of the vapor deposited alloy constituents for the TFT are reported in this study. K-type (chromel and alumel) thermocouple wires were used as targets for physical vapor deposition of the component layers of the TFT. The calibration of the TFT using high-speed data acquisition is reported. The calibration curves of TFT packaged using ultrasonic wire bonding of Al wires are compared with TFT packaged using resistance arc welding of K-type thermocouple wires. TFT packaged using resistance arc welding is found to have better temperature response under steady-state conditions.

Index Terms—Interconnects, resistance arc welding, thin film thermocouples (TFTs), wire bonding, X-ray photoelectron spectroscopy (XPS).

I. INTRODUCTION

THE need to study microscale thermal phenomena on heated surfaces in multiphase flows with high spatial and temporal resolution necessitates the development of miniaturized thermography devices with fast response times. Such thermography devices also have potential applications in thermal management systems for high heat flux devices (e.g., electronic chip cooling and materials processing). The ever shrinking feature sizes in the microelectronics industry have created situations where large amounts of heat are generated

in very small areas (e.g., ITRS 2006 Update [1]). Thermal inefficiencies can seriously degrade the electronic performance of these devices. Therefore, accurate, fast, and seamless monitoring is beneficial for efficient thermal management of high-performance electronic devices. In such applications, arrays of integrated miniaturized sensors on chips and packages can provide an accurate measure of device performance without interfering with the functioning of the device circuitry. Submillimeter scale thermography techniques are also required for studying the scale effects in transport mechanisms for fluid flows, particularly in multiphase flows. Optical thermography techniques are often not amenable for studying multiphase flows due to optical interference from the constituent phases.

Conventional techniques for submillimeter scale thermography reported in literature for multiphase flows include: liquid crystal thermography [2]–[6], radiation thermography [7]–[12], and embedded wire bead thermocouples [13], [14].

Various techniques reported in micromachining literature for fabricating temperature sensors were summarized by Kovacs [14]. These include: 1) resistance temperature detectors (RTD); 2) thermistors; 3) junction temperature sensors (JTS), e.g., diode or complementary metal–oxide–semiconductor (CMOS) (transistor) temperature sensors; and 4) doped semiconductor temperature sensors. Fabrication of polysilicon resistance temperature detectors (RTDs) were reported by Wang *et al.* [15], for studying jet impingement and spray cooling studies. In general, RTD and thermistors suffer from nonlinearity, self-heating, drift, parasitic contribution from interconnects, low resolution, complicated signal analysis, etc. These effects can increase measurement uncertainty, compromise precision/accuracy, require elaborate data acquisition schemes, and necessitate sophisticated signal conditioning paraphernalia for the experimental apparatus. JTS sensors provide the most superior performance, however, the fabrication steps for these sensors can be quite elaborate.

Apart from these considerations mentioned above, sensor speed can also be a crucial factor, especially for studying micro/nanoscale transport phenomena where the desired response speeds can be in the kilohertz to megahertz range. Liquid crystal thermography and radiation thermography have enabled the sensor response speeds of the order of hertz. Embedded wire bead thermocouples can provide response speeds ranging from 1 to ~ 10 Hz. Also, the size of the wire beads can potentially interact with the microscale transport mechanisms, when they are placed directly on the heated surface for measuring surface temperature transients.

Manuscript received April 27, 2006; revised June 06, 2007. Current version published July 22, 2009. This work was supported in part by the “New Investigator Program” (NIP 2005) of the Texas Space Grants Consortium (TSGC), the Texas Engineering Experimentation Station (TEES), and the Mechanical Engineering Department (New Faculty Start-Up Grant) at Texas A&M University. This work was recommended for publication by Associate Editor S. Bhavnani upon evaluation of the reviewers comments.

N. Sinha is with the Mechanical Engineering Department, University of Pennsylvania, Philadelphia, PA 19104 USA.

H.-S. Ahn and D. Banerjee are with the Mechanical Engineering Department, Texas A&M University, College Station, TX 77843 USA (e-mail: dbanerjee@tamu.edu).

R. Williams was with the Mechanical Engineering Department, Texas A&M University, College Station, TX 77843 USA. He is now with Nuventix.

Color versions of one or more of the figures in this paper are available online at <http://ieeexplore.ieee.org>.

Digital Object Identifier 10.1109/TCAPT.2009.2013982

The unsophisticated fabrication process, the simplicity of supporting apparatus, and the ability to seamlessly interface with standard high-speed data acquisition instruments led to the current study for developing thin film thermocouples (TFTs). In contrast to the conventional wire-bead metal junction thermocouples, these thermocouples were fabricated using physical vapor deposition of dissimilar metals and the “liftoff” surface micromachining technique, similar to the technique used by Chu *et al.* [29] and Chu *et al.* [30]. More information on micromachining processes can be obtained from [14]. The small size of the sensing elements can enable sensing speeds from kilohertz to megahertz.

The K-type thermocouple arrays reported in this study consist of thin films of chromel and alumel alloys (which are a few hundred nanometers in height and tens of micrometers in width). The TFTs were microfabricated on silicon and Pyrex[®] substrates. An advantage of the reported technique is that the designed width can be scaled down to submicron feature sizes using appropriate lithography steps, if required.

The concept of thin film thermocouples was first reported in the 1930s by Marshall *et al.* [16]. Various combinations of thermocouple elements have been studied and analyzed by Marshall *et al.* [17]. TFTs have been used for various surface temperature measurements by Bullis [16], Assanis *et al.* [18], Debey *et al.* [19], Tian *et al.* [20], and Laugier [21], due to their inherent advantages over wire-bead-type thermocouples. The use of thin films for surface temperature measurement provides the advantage that they can be fabricated on surfaces where placing of beaded thermocouple might interfere with the functioning of the object, e.g., aerodynamic structures where the surface roughness is of extreme importance and cannot be compromised. TFTs have extremely small thermal inertia when compared to conventional beaded thermocouples. This results in a fast thermal response, as reported by Chu *et al.* [30]. The small metal volume also causes minimal interference of the surface temperature distribution, as stated in [29]. Numerical simulations for studying the effects/distortions caused by the presence of thin film thermocouples on surfaces were done by Tian *et al.* [20] and the presence of TFT was found to have minimal effect on the surface temperature distribution. Bullis [17] reported that TFTs provide more accurate measurement of surface temperatures than beaded thermocouples. Hence, we expect better performance from these thermocouples in terms of sensitivity, accuracy, speed, and linearity of response.

A thorough understanding of surface thermal transients during phase change processes is yet to be achieved. This is especially useful for various cooling applications (e.g., immersion cooling). The TFTs described in this study were developed to study surface temperature fluctuations in boiling and multiphase flows primarily for their fast response (high temporal resolution ~ 10 nanoseconds) and for incorporation in high spatial density architectures (high spatial resolution ~ 500 nm $-10\text{-}\mu$ pitch). The small footprint and elemental volumes of the thermocouple junctions provide the ability to measure minute fluctuations which may not be detectable by a conventional wire-bead thermocouple. Park *et al.* [22] fabricated an array of T-type thin film thermocouples to measure temperature in a 1 cm \times 1 cm area. The material choice of TFT

in elevated temperature applications is guided by the possibility of intermetallic interactions and environmental interactions, as described by Kreider *et al.* [23] and Kreider *et al.* [24].

Packaging is widely acknowledged to be the most difficult step of microfabrication and often the limiting step in commercialization of microdevices. After the fabrication of TFT's, obtaining the temperature response in an accurate and practical manner proved to be a formidable task. In this paper, we report the various methods we explored for packaging the TFT. Since the homogeneity of material composition used for packaging the TFT affects the calibration and performance of TFT, this was one of the primary concerns. Therefore, packaging (primarily interconnect fabrication) is crucial for reliable performance and ensuring measurement accuracy of TFT. The solution to this packaging problem has been reported in the literature in the form of parallel gap welding by Holanda *et al.* [25] and spot welding by Zupan *et al.* [26].

In this study, we report an alternative approach using resistance arc welding of thin chromel and alumel wires (125- μ diameter) on corresponding bond pads. We compare the performance of TFT packaged using homogeneous interconnects (resistance arc welding) with heterogeneous interconnects (wire bonding of aluminum wires of 25- μ diameter). Since the temperature range of interest is from 50 °C to 200 °C, K-type TFTs were chosen for this study. As mentioned before, the target applications for these TFT are for seamless monitoring of thermal response of high-performance electronic devices (monitoring nonuniformity of temperature distribution on device packages or “hot spots”) and investigating submillimeter scale thermal transport mechanisms in multiphase flows. Pool boiling curve was obtained using the TFT and is reported in this study.

II. FABRICATION

A. Microfabrication of Thin Film Thermocouples

For the microfabrication of K-type TFTs, conventional photolithography and metal vapor deposition processes were used. Two separate photomasks were used for patterning of the chromel and alumel metal lines. Pairs of dissimilar metal lines (50–100 μ wide) overlapped near the center of the mask to form an array of thermocouple junctions. The metal lines terminated in arrays of paired and square sized bond pads at the periphery of the masks. Four alignment marks at the four corners of the photomasks were designed in the mask layout for aligning the thermocouple junctions during photolithography steps (Fig. 1).

A Quintel Q4000 mask aligner was used to perform contact lithography. Shipley-1827 photoresist (Rohm and Haas Electronic Materials, Philadelphia, PA) was used for spin coating on SCS P6204 nonprogrammable spin coater. The photoresist thickness was 2–2.5 μ m after running the spin coater for 60 s at a spin speed of 3000 r/min. The spin coated wafers were exposed using an UV lamp at a lamp power of approximately 300 W, using the Quintel mask aligner. Exposure times varied from 8 to 15 s. The exposed wafers were developed using Microposit MF-319 developer (by Rohm and Haas Electronic Materials). A plasma de-scum was performed using oxygen plasma on a march plasma systems model CS-1701 reactive ion etcher for 10 s. BOC Edwards Auto 306 (Mississauga, ON,

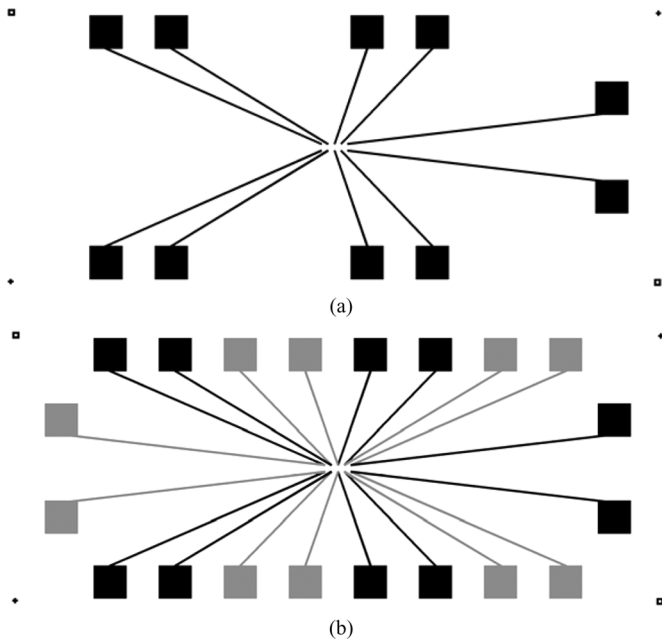


Fig. 1. (a) Mask layout for a single conductor layer showing the metal traces, bond pads (1 mm^2), and alignment marks on the four corners. (b) Mask layouts for the two conductor layers in aligned and overlapped position, showing the formation of the thermocouple junctions.

Canada) metal evaporation chamber was used for deposition of chromel (+) and alumel (-). Alloy wires of chromel (Ni: 90% and chromium: 10%) and alumel (Ni: 95% and aluminum: 5%) obtained from Omega Engineering, Inc. (Stamford, CT), were used as targets. (These wires are used for fabricating the conventional wire-bead thermocouples.) The deposition thickness varied from 220 to 270 nm for each of the thermocouple element layers. The choice of deposition thickness was guided by the minimum thickness required to suitably reproduce the bulk thermal Seebeck coefficients, as reported by Marshall *et al.* [16]. An adhesion layer of chromium of 20-nm thickness was initially deposited prior to the deposition of the chromel or the alumel layers (similar to [30]). Liftoff process was performed using either acetone or nano remover PG (Micro Chem Corporation, Newton, MA). The photolithography and liftoff process were separately repeated for both conducting layers (chromel and alumel). Fig. 2(a) shows an image of the fabricated TFT observed under an optical microscope. Fig. 2(b) shows a scanning electron microscope (SEM) image of the TFT. Fig. 2(c) shows a picture taken by using a microscope, showing all the ten alumel–chromel junctions of the array. NanoTM Remover PG (manufactured by Micro Chem Corporation) was used to remove the photoresist during the liftoff process.

B. Metal Composition Analysis After Deposition

A Kratos axis ultra imaging X-ray photoelectron spectrometer (XPS) was employed to analyze the composition of the deposited metal traces of the TFT. Two separate test substrates were used during the consecutive vapor deposition steps of the chromel and alumel layers. The substrates were loaded into the XPS instrument and the compositions of the deposited metal surfaces were analyzed. The spectrum of elements in the samples obtained from XPS measurements is plotted in Fig. 3 (alumel). The spectral data shown in Fig. 3 was used

to obtain the composition of the component of the TFT. The figure displayed here shows the survey curve (the curve which shows all the elements that are present on the surface) for one of the fabricated samples. The peaks shown here are indicative of the presence of the constituent elements. The composition can be obtained by comparing the energies of these peaks with the known standard energies of ejected electrons from various elements in XPS.

Table I shows the composition analyses of the TFT component layers (chromel and alumel), measured using XPS for the two samples. The measured values show that the composition of the deposited layers is significantly different from the composition of the target (reported by the manufacturer). These measurements show that the fabricated TFT can potentially have a different thermoelectric response compared to conventional K-type thermocouples (used as the target material). Hence, the TFT thermal response was calibrated using standard wire-bead K-type thermocouples as reference under thermal steady-state conditions.

The deposited metal layers have a different composition compared to the target possibly due to the different values for vapor pressures of the constituent metals, partial pressures (including leaked gasses in the chamber), and vapor diffusivities in the physical vapor deposition chamber for the component metals (Ni, Cr, and Al). Although sputtering provides better conformity of the composition of the deposited alloy to the target (compared to physical vapor deposition), it is also more expensive process requiring specialized metal (or alloy) targets for the deposition process. However, the biggest disadvantage of sputtering over physical vapor deposition during liftoff process is the step coverage. The processing steps used for microfabrication of TFT in this study involve the liftoff process. The solvent used for liftoff process is NanoTM Remover PG (manufacturer: Micro Chem Corporation). The better step coverage from sputtering process impedes liftoff. Fig. 4 schematically shows the two cases, i.e., physical vapor deposition and sputtering. For improving the speed and yield during the liftoff process, the photoresist remover solution needs to come in contact with the photoresist. By virtue of better step coverage, sputtering hinders this contact and is thus not a suitable process when liftoff is required. Hence, physical vapor deposition was chosen for microfabrication of TFT.

III. PACKAGING

Several interconnect fabrication strategies were explored, including pressure contacts, wire bonding (of aluminum wires), and resistance arc welding. These are reported below.

A. Wire Bonding

Wire bonding, explained in [27], is conventionally used for packaging of interconnects in microelectronics. However, this technique is limited to low melting point materials such as gold and aluminum wires. Wire bonding of chromel and alumel wires of 25- and 75- μm diameter was explored on a Kulicke & Soffa, Ltd. (Fort Washington, PA), 4523A digital manual wire/wedge bonder. Since these alloys melt at substantially higher temperatures than gold or aluminum, successful wire bonding could not be achieved with chromel and alumel wires. Hence, aluminum



Fig. 2. (a) Optical microscopy image of TFT junction (observed in the wire bonder instrument). (b) SEM Image of TFT junction showing two TFT junctions formed by overlapping the two conductor layers (chromel and alumel). (c) Image taken using a microscope, showing all the ten junctions (alumel–chromel junctions) of the array.

wires ($25\text{-}\mu\text{m}$ diameter) were initially used for wire bonding on the microfabricated bond pads. The parameter values used for successful wire bonding of aluminum wire were: vertical feed (90°), power setting of 2.62, time setting of 2.0, and force setting of 1.4. Since the bond strength was weak, subsequently wire bonding was performed with a thicker bond wire ($75\text{-}\mu\text{m}$ diameter). The heterogeneity in thermocouple material composition at the bond pad due to packaged interconnects resulted in parasitic junction potentials being introduced into the sensor element. These parasitic junctions interfered with successful thermography operations. This is described in more detail in Section IV.

B. Resistance Arc Welding Method

In conventional resistance arc welding method, explained in [28], an arc is sustained in a small gap between an electrically conducting substrate that is brought in close proximity to a wire

held at a high electric potential. The heat generated from the arc melts the tip of the wire. The melted tip subsequently cools by losing heat to the ambient and solidifies to form a physical bond between the wire and the substrate. After comparing the aforementioned strategies for packaging of interconnects, resistance arc welding was explored for bonding of the chromel and alumel wires to the bond pads. The size of the microfabricated bond pads was $1\text{ mm} \times 1\text{ mm}$ and the wires were melted onto the bond pad. Initially, a direct current (dc) supply ($0\text{--}340\text{ V}$, $0\text{--}0.1\text{ A}$) was explored, as arcs produced using dc sources are known to have better bonding characteristics, as described in [28]. The dc source produced considerable arcing. However, the low current rating of the dc power supply was an impediment to continued use of the instrument. Hence, the use of an alternating current (ac) supply was explored subsequently. An especially tailored method for small scale resistance arc welding was used. A standard variable transformer by Staco Energy Products Co.

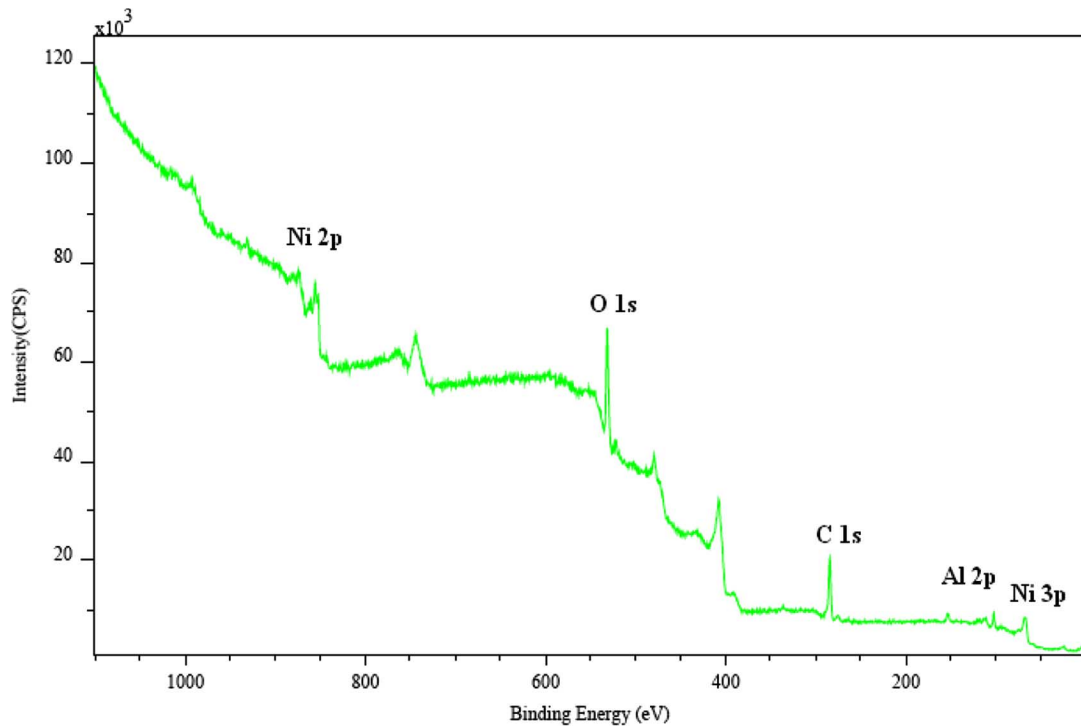


Fig. 3. Graph generated by XPS showing the spectrum of elements on the surface of Alumel. Ni 2p+ Ni 3p (84.32%) and Al 2p (15.68%). (% mass concentration.)

TABLE I
COMPOSITION ANALYSES OF TFT LAYERS (USING XPS)

Concentration	Alumel				Chromel			
	Atomic Concentration %		Mass Concentration %		Atomic Concentration %		Mass Concentration %	
Composition	Ni	Al	Ni	Al	Ni	Cr	Ni	Cr
Sample 1	66.52	33.47	81.22	18.77	78.85	21.15	80.8	19.2
Sample 2	71.17	28.82	84.32	15.68	76.4	23.6	78.52	21.48
Target	95	5	95	5	90	10	90	10

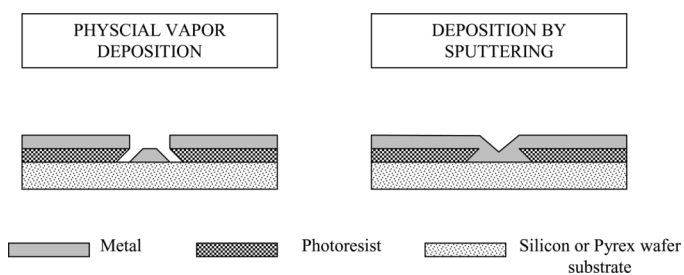


Fig. 4. Schematic showing better step coverage obtained by sputtering of metal thin films compared to physical vapor deposition. Better step coverage impedes liftoff process used for microfabrication of the TFTs.

(Dayton, OH) with an input: 120 V 50/60 Hz, output: 0–120/140 V, and a rating of 0.7 kVA (kilovolt ampere) with 5 A was used. A 3-A slow blow fuse was connected in series with the transformer input for safety.

In an initial strategy, the edge of the wire tip (to be welded) was bent and positioned parallel to the bond pad surface (Fig. 5). This strategy of bending the wire was designed to obtain multiple arcs in a single bonding attempt and to obtain multiple melt zones, and therefore, a stronger bond. In this strategy, the current

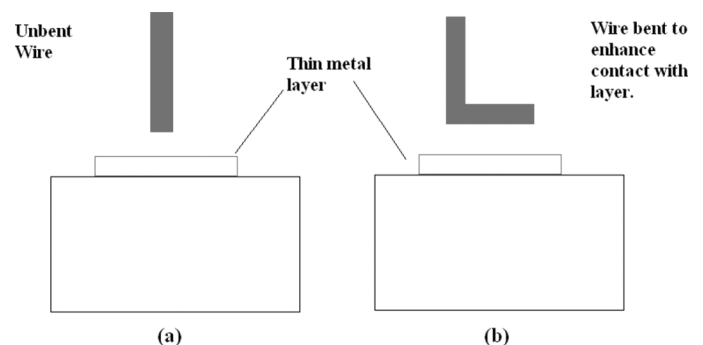


Fig. 5. Schematic showing two strategies for resistance arc welding. (a) A straight wire is used to strike an arc by bringing it in close proximity with the bond pad. (b) A bent wire is used to simultaneously strike multiple arcs by bringing it in close proximity with the bond pad.

was passed through the whole length of the wire which caused it to glow red hot momentarily during arc welding.

This method was subsequently modified by using two different diameter wires (125 and 500 μm). The thick (500- μm diameter) wires were attached to the 125- μm diameter wires of the same kind (chromel or alumel) using a thermocouple welder. A pair of thicker wires (~ 1 cm long) was mounted

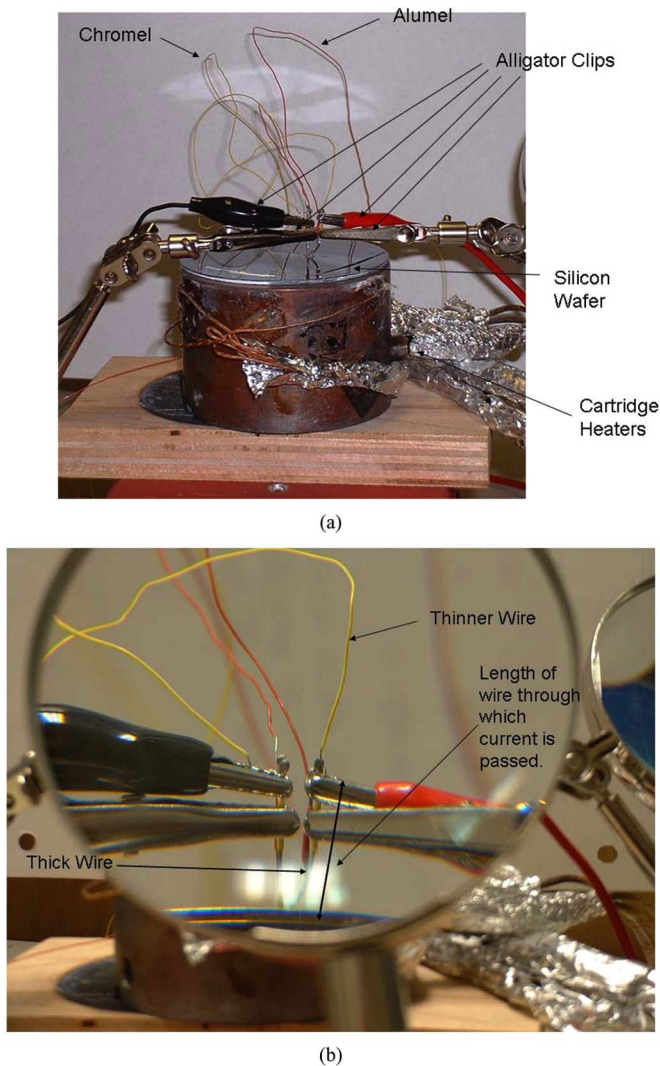


Fig. 6. (a) Photograph showing a pair of crocodile clips used to position the thick wires (500 μ) over the bond pads and to pass current through the thick wire. (b) Enlarged view of the setup.

separately on a pair of metal alligator clips. The thicker wires were then placed at a similar level while in close vertical proximity (~ 1 mm) to a bond pad of the same material (chromel or alumel). The wires were placed in a manner without contacting each other or the bond pad. Another pair metal alligator clips were mounted on the back side (i.e., top portion) of the thicker wires and were connected separately using copper wires to the two leads of the transformer for supplying the current required for arc welding. Current was, therefore, passed through a small portion of the thicker wires that were mounted on the alligator clips. The electrical current was, therefore, not passed through the thinner wire but through the TFT elements during the arc welding. Fig. 6(a) and (b) illustrates this apparatus. Prior to striking an arc, the thicker wires were first cleaned at the bare ends using as 400 grit sandpaper to remove the surface contaminants. The thicker wires were then bonded to the bond pad of similar material (chromel or alumel) by striking an arc at each bond pad. The silicon wafer substrate (containing the surface micromachined TFT and the bond pads) was placed on a

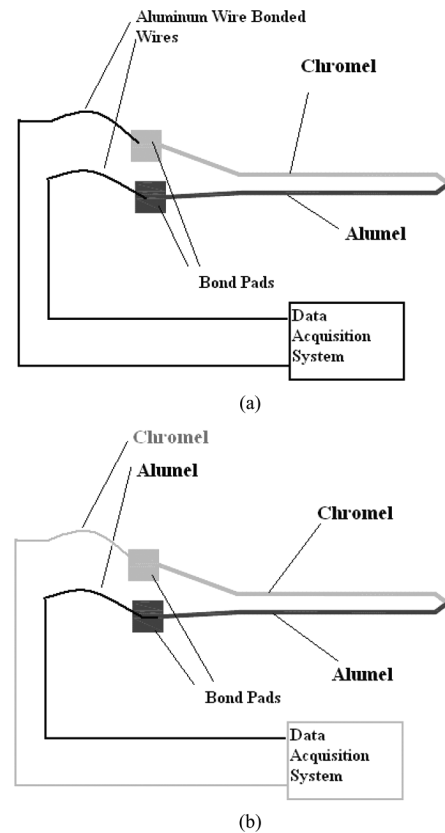


Fig. 7. (a) Schematic showing the connection between the TFT bond pads and the data acquisition system using wire bonding of aluminum wires. (b) Schematic showing the connection between the TFT bond pads and the data acquisition system using resistance arc welding technique to bond chromel and alumel wires.

multijack. The multijack was raised slowly to progressively decrease the gap between the wafer and the wire tip for striking an electric arc. Immediately after the electric arcs caused the bare ends of the thicker wires to melt and adhere to the bond pads, the transformer was switched off (within seconds). The voltage drop in the weld was approximately 30% of the maximum voltage (~ 36 V). Great care was taken to avoid the wires from touching each other and from arcing to form a bond among the wires. Once the weld was formed, an epoxy (JB Weld, Sulphur Springs, TX) was dispensed over the welds to provide additional mechanical strength.

IV. RESULTS AND DISCUSSION

A. Calibration

TFTs were fabricated using the process of metal evaporation. As mentioned in Section II, this causes the composition of the deposited metal to be different from the target material. To ensure conformity of temperature response of the fabricated TFT, a standard calibration procedure was followed.

To calibrate the fabricated TFT, an experimental apparatus was constructed. The experimental apparatus consisted of a copper block (99.99% pure, deoxidized) with embedded cartridge heaters and the wafer. The wafer (containing the microfabricated TFT) was mounted on the copper block. A

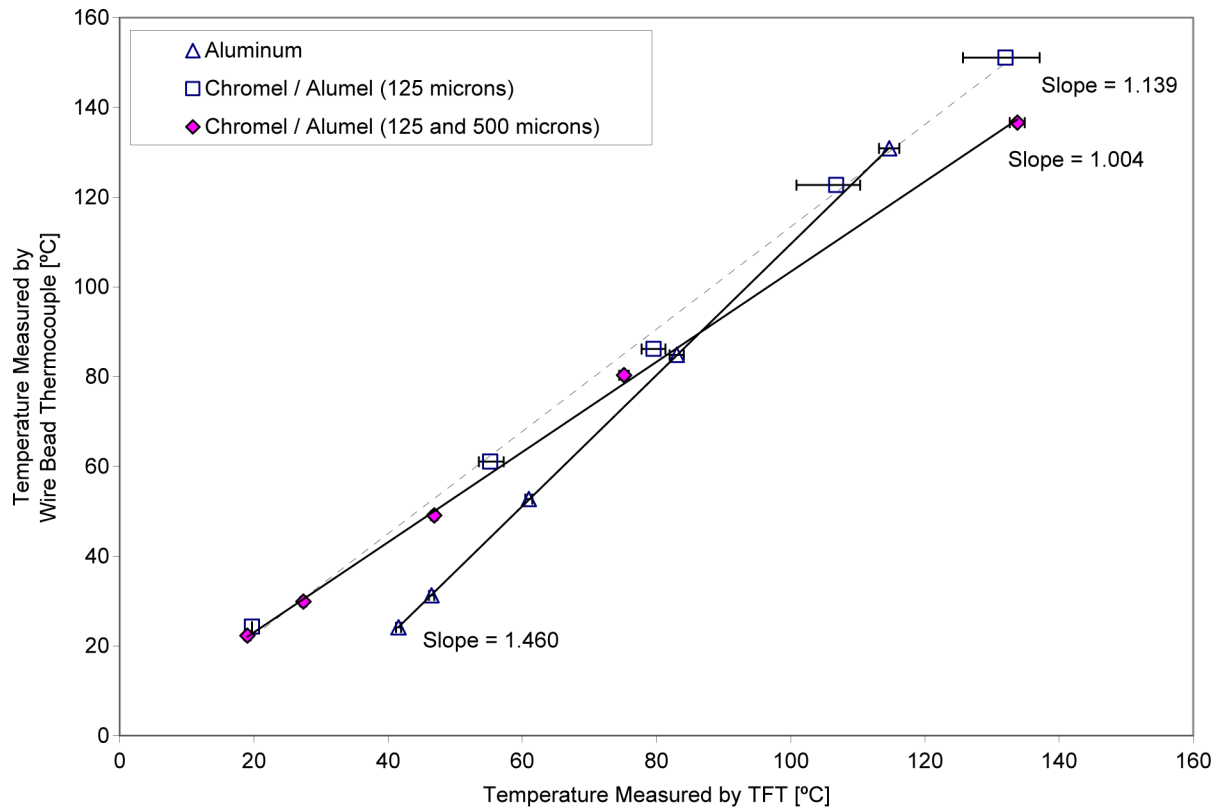


Fig. 8. Calibration curve of TFT packaged by wire bonding using (a) aluminum wires ($75\text{-}\mu$ diameter), slope = 1.46; (b) chromel and alumel wires ($125\text{-}\mu$ diameter), slope = 1.14; and (c) chromel and alumel wires (125- and $500\text{-}\mu$ diameter), slope = 1.0. A standard wire-bead K-type thermocouple (chromel/alumel wires) is used as a reference for the calibration. The slope of the best fit line for the calibration curve is shown by the various straight lines.

standard wire-bead K-type thermocouple was attached on the surface of the wafer [shown in Fig. 6(a)]. The wire-bead K-type thermocouple was previously calibrated against the National Institute of Standards and Technology (NIST) calibrated mercury thermometer. The wafer containing the packaged TFT array and the attached wire bead thermocouple was placed on the copper block heater experimental apparatus. Silicone paste (Dow Corning[®], Midland, MI, 340 heat sink compound) was applied uniformly between the wafer and the copper block. The silicone layer acts as an upstream thermal resistance that affects both the TFT and the wire-bead thermocouples in similar manner. Hence, the calibration results were unaffected due to the application of the silicone paste. Difference in temperature readings due to anomalous heat loss issues were eliminated by placing the wire bead thermocouple in close proximity to the TFT (less than 1 cm apart).

The current passing through the heaters (embedded in the copper block) was controlled by a variable transformer (type 1010, input 120 V 50/60 Hz, output 0–120/140 V, 10 A, 1.4 kVA by Staco Energy Products Co.). Both the wire bead thermocouple and the TFT were connected to the data acquisition system (National Instruments, Austin, TX, PCI 6204E, 200 kS/s, 12-b, 16 analog multifunctional DAQ using SCXI 1000 (Chassis) and TC-2095 terminal block). The schematic for connection to the data acquisition system is shown in Fig. 7(a) and (b). The variable transformer was set to a pre-determined voltage and the apparatus was allowed to reach steady state. At the steady state, the values of both the ther-

mocouples (TFT and wire-bead thermocouple) were recorded using the data acquisition system and the calibration curve was constructed at different temperatures from 20 °C to 140 °C. The results of the calibration are presented in the following paragraphs.

Fig. 8 shows the calibration curve for the TFT packaged by wire bonding using the three techniques. The measurements show a nearly linear response for the TFT packaged using wire bonding of aluminum wires. The slope of the calibration line is close to 1.46 for ultrasonic wire bonding using aluminum. As described earlier, the presence of aluminum in the measuring circuit creates a parasitic junction. To account for the parasitic junction potential at the bond pads the bond pad temperature would be required. In the absence of such data, larger errors can be introduced, especially for transient measurements. So, even if the calibration response is linear, the actual performance of the aluminum wire bonded TFT can be nonlinear in certain situations where the two bond pads are at a different temperature compared to the TFT junctions. Since such nonuniformities in temperature are difficult to compensate for, measurement errors will occur.

Similar calibration measurements were performed for the TFT which were packaged using resistance arc welding technique using chromel and alumel wires. Fig. 8 displays the calibration data for TFT that were packaged by using a single wire that was bent parallel to the bond pad. The response of the TFT is found to be linear with a slope of 1.139. Fig. 8 displays the calibration data for TFT packaged using K-type

thermocouple wires (chromel or alumel) of two different diameters. The slope of the calibration curve is 1.004. This shows that the effects due to the parasitic junction potentials at the bond pads are eliminated and the temperature response of the packaged TFT closely follows the response of a standard K-type wire-bead thermocouple.

Comparing the three trend lines in Fig. 8, it can be observed that the calibration curve of TFT packaged using arc welding has better linearity and slope closer to unity. This shows that the latter packaging strategy (arc welding) results in temperature measurements, which match those from standard K-type thermocouples. Following the calibration experiments, one of the bonds obtained by resistance arc welding was used for destructive testing to understand the mechanical failure mode for the bonds. For performing this test, the wire was pulled from the bond. It was found that the thermocouple wire broke off at the top of the deposited metal, while leaving the deposited metal intact. This shows that the adhesive strength of the bond is larger than the breaking strength of the thermocouple wire.

V. CONCLUSION

Different techniques for fabrication and packaging of microthermocouples were explored. The use of resistance arc welding of thermocouple wires (chromel and alumel) was found to be a better method for packaging of K-type TFTs than ultrasonic wire bonding using aluminum. Welding helps in maintaining material homogeneity and ensuring better temperature response. It is found that conventional ultrasonic wire bonding of aluminum results in material inhomogeneity during the packaging step and leads to the creation of a parasitic junction which degrades the temperature response of the TFT. Better bond strength is achieved by bending the tip of the wire to obtain multiple arcs, which in turn causes a larger melt zone (and bonding area) on the wires. However, this strategy can cause the connecting wires to be heated to high temperatures probably resulting in partial oxidation of the wires. Using a contraption of wires of two different diameters was found to yield the best packaging performance. The TFTs were successfully implemented in pool boiling experiments and were used to obtain the boiling curve for nucleate boiling. Fast Fourier transform (FFT) analyses of the temperature transients were performed at different superheats. The FFT analyses were used to demonstrate the existence of higher frequency temperature transients in boiling that can be correlated to bubble departure frequency and formation of microscale cold spots in pool boiling. Further investigations are underway using the TFT developed in this study. The packaging techniques developed in this study can be utilized for improving the reliability of microscale temperature measurements for phenomenological studies of pool boiling. The enhanced understanding of these transport processes can be utilized to develop next generations of heat transfer augmentation schemes.

ACKNOWLEDGMENT

The authors would like to thank Dr. S. Lau at Texas A&M University, for access to laboratory equipment. They would also like to thank Y. Ramirez at the Heat Transfer Laboratory,

Texas A&M University, for his help. The authors would like to thank Dr. V. Ugaz at Texas A&M University for helpful suggestions. They would also like to thank Dr. W. Lackowski (former Manager), Y. Vasilyeva (Research Assistant), and S. Chatterjee (former Research Assistant) at the Center for Integrated Micro-Chemical Systems/Materials Characterization Facility (CIMS/MCF), Texas A&M University for helpful support.

REFERENCES

- [1] International Roadmap for Semiconductors, ITRS 2006 Update [Online]. Available: www.itrs.net/reports.html
- [2] D. B. R. Kenning and Y. Yan, "Pool boiling heat transfer on a thin plate: Features revealed by liquid-crystal thermography," *Int. J. Heat Mass Transfer*, vol. 39, pp. 3117–3137, 1996.
- [3] D. B. R. Kenning, "Liquid crystal thermography as a tool for investigating the development of boiling," in *Proc. Eng. Found. Conf. Pool External Flow Boiling*, Santa Barbara, CA, Mar. 22–27, 1992, pp. 79–82.
- [4] D. B. R. Kenning, "Wall temperature patterns in nucleate boiling: Spatial and temporal variations," in *Proc. 9th Int. Heat Transfer Conf.*, Jerusalem, 1990, vol. 3, pp. 33–38.
- [5] J. H. Ellepola and D. B. R. Kenning, "Nucleation site interaction in pool boiling," in *Proc. 2nd Eur. Thermal Sci./14th UN Nat. Heat Transfer Conf.*, Rome, Italy, May 29–31, 1996, pp. 1669–1675.
- [6] J. H. Ellepola, P. E. Sharry, and D. B. R. Kenning, "Is nucleate boiling chaotic? (who cares)," in *Proc. Eurotherm 48, Pool Boiling*, Paderborn, Germany, 1996, pp. 17–24.
- [7] M. Shoji, T. Kohno, J. Negishi, S. Toyoshima, and A. Maeda, "Chaos in boiling on a small size heater," in *Proc. 4th ASME-JSME Thermal Eng. Joint Conf.*, 1995, vol. 2, pp. 225–232.
- [8] M. Shoji, M. Maeda, and S. Fujii, "Non-linear bubble dynamics," in *Proc. 32nd Jpn. Nat. Heat Transfer Conf.*, Yamaguchi, Japan, 1995, vol. 1, pp. 257–258.
- [9] M. Shoji and Y. Takagi, "Bubbling features from a single artificial cavity," *Int. J. Heat Mass Transfer*, vol. 44, pp. 2763–2776, 2001.
- [10] M. Shoji and L. Zhang, "Boiling on an artificial surface—Bubbling features and nucleation site interactions," in *Proc. 20th UIT Nat. Heat Transfer Conf.*, Maratea, Italy, Jun. 27–29, 2002, pp. 37–42, 2002.
- [11] L. Zhang and M. Shoji, "Nucleation site interactions in pool boiling—Experimental study by employing artificial boiling surface," in *Proc. 5th ASME-JSME Thermal Eng. Joint Conf.*, Mar. 16–20, 2003, pp. 15–20.
- [12] Y. M. Qiao and S. Chandra, "Boiling droplets on a hot surface in low gravity," *Int. J. Heat Mass Transfer*, vol. 39, pp. 1379–1393, 1996.
- [13] Y. Hamamura, "Heat flux fluctuation on steady state transition boiling," in *Proc. 4th ASME-JSME Thermal Joint Conf.*, 1995, vol. 2, pp. 209–214.
- [14] G. T. A. Kovacs, *Micromachined Transducers: Sourcebook*. New York: WCB/McGraw Hill, 1998.
- [15] E. N. Wang, L. Zhang, L. Jiang, J.-M. Koo, J. G. Maveety, E. A. Sanchez, K. E. Goodson, and T. W. Kenny, "Micromachined jets for liquid impingement cooling of VLSI chips," *IEEE J. Microelectromech. Syst.*, vol. 13, no. 5, pp. 833–842, Oct. 2004.
- [16] R. Marshall, L. Atlas, and T. Putner, "The preparation and performance of thin film thermocouples," *J. Sci. Instrum.*, vol. 43, pp. 144–149, 1966.
- [17] L. H. Bullis, "Vacuum-deposited thin-film thermocouples for accurate measurement of substrate surface temperature," *J. Sci. Instrum.*, vol. 40, pp. 592–593, 1963.
- [18] D. N. Assanis and F. A. Friedmann, "A thin film thermocouple for transient heat transfer measurements in ceramic-coated combustion chambers," *Int. Commun. Heat Mass Transfer*, vol. 20, pp. 458–468, 1993.
- [19] D. Debey, R. Bluhm, N. Habets, and H. Kurz, "Fabrication of planar thermocouples for real-time measurements of temperature profiles in polymer melts," *Sensors Actuators A*, vol. 58, pp. 179–184, 1997.
- [20] X. Tian, F. E. Kennedy, J. J. Deacutis, and A. K. Henning, "The development and use of thin film thermocouples for contact temperature measurement," *Tribology Trans.*, vol. 35, pp. 491–499, 1992.
- [21] M. Laugier, "The construction and use of thin film thermocouples for the measurement of surface temperature: Applications to substrate temperature determination and thermal bending of a cantilevered plate during film deposition," *Thin Solid Films*, vol. 67, pp. 163–170, 1980.
- [22] J.-J. Park and M. Taya, "Design of micro-arrayed thin film thermocouples (TFTC)," in *Proc. IPACK*, Jul. 6–11, 2003.

- [23] K. G. Kreider and F. DiMeo, "Platinum/palladium thin-film thermocouples for temperature measurements on silicon wafers," *Sensors Actuators A*, vol. 69, pp. 48–52, 1998.
- [24] K. G. Kreider and G. Gillen, "High temperature materials for thin-film thermocouples on silicon wafers," *Thin Solid Films*, vol. 376, no. 1, pp. 32–37, Nov. 2000.
- [25] R. Holanda, W. S. Kim, E. Pencil, M. Groth, and G. A. Danzey, "Attachment of lead wires to thin film thermocouples mounted on high temperature materials using the parallel gap welding process," in *NASA Tech. Memorandum 102442 for 177th Meeting Electromech. Soc.*, Montreal, QC, Canada, May 6–11, 1990.
- [26] M. Zupan, M. J. Hayden, C. J. Boehlert, and K. J. Hemker, "Development of high temperature microsample testing," *Experimental Mech.*, vol. 41, no. 3, Sep. 2001.
- [27] G. G. Harman, *Wire Bonding in Microelectronics: Materials, Processes*, 2nd ed. New York: McGraw Hill, 1997.
- [28] R. F. Beard, "Basics of GMAW and GTAW: Gas metal arc welding, gas tungsten arc welding," *Amer. Assoc. Vocat. Instruction*, 1999, ISBN: 0896062864.
- [29] D. Chu, D. T. Bilir, R. Fabian, W. Pease, and K. E. Goodson, "Submicron thermocouple measurements of electron-beam resist heating," *J. Vac. Sci. Technol.*, vol. B20, no. 6, pp. 3044–3046, Nov./Dec. 2002.
- [30] D. Chu, D. T. Bilir, R. Fabian, W. Pease, and K. E. Goodson, "Thin film nano thermocouple sensors for application in laser and electron beam irradiation," in *Proc. 12th Int. Conf. Solid State Sensors Actuators Microsyst.*, Boston, MA, Jun. 8–12, 2003, pp. 1112–1115.



Nipun Sinha received the B.E. degree in mechanical engineering from Punjab Engineering College, Chandigarh, India, in 2004 and the M.S. degree in mechanical engineering from Texas A&M University, College Station, for which he performed research at the Multi-Phase Flow and Heat Transfer Laboratory. Currently, he is working towards the Ph.D. degree in mechanical engineering at the University of Pennsylvania, Philadelphia.

He has worked at Indian Institute of Technology (IIT), Delhi, India, and at Indian Oil Corporation Research and Development Centre, Faridabad, India, as a Research Trainee. His research interests include nano/microfabrication processes, surface characterization techniques, MEMS, boiling, heat transfer, fluid mechanics, and bio/nanotechnology.



Hee Seok Ahn was born in Seoul, Korea, in 1965. He received the B.S. and M.S. degrees in mechanical engineering from Korea University, Seoul, Korea, in 1988 and 1990, respectively, and the Ph.D. degree in mechanical engineering from Texas A&M University, College Station, in 2006, for which he performed research at the Multi-Phase Flow and Heat Transfer Laboratory and the Heat and Mass Transfer Laboratory.

Between 1996 and 2002, he was a Senior Research Engineer at Hyundai Motor Company in Korea. He

published several papers, which include "Micro-machined temperature sensor arrays for studying micro-scale features in film boiling," "Analysis of EGR distribution characteristics in intake manifolds and plenum chamber with 1-D and 3-D hybrid calculations," and "Development of HMC axially stratified lean combustion engine." His research interests include microscale heat transfer in boiling, convective heat and mass transfer, electronic cooling, turbine and automotive engine cooling, microfabrication, and computational fluids dynamics (CFD).

Dr. Ahn has been a member of the Society of Automotive Engineers (SAE) since 1992.



Randall Williams received the B.S. degree in mechanical engineering from Texas A&M University, College Station, where he was an undergraduate student researcher at the Multi-Phase Flows and Heat Transfer Laboratory.

Currently, he is a Design Engineer for Nuventix, Austin, TX. His primary interests for technology development include CFD and mechanical modeling of synthetic jet systems.



Debjyoti Banerjee received the B.S. in technology (honors) from Indian Institute of Technology (IIT), Kharagpur, India, in 1992, three M.S. degrees and the Ph.D. degree in mechanical engineering from the University of California at Los Angeles (UCLA, with minor in MEMS), in 1999.

He worked as a Manager of Fluidics and Device Engineering Group in the Advanced Research & Technology (ART) division at Applied Biosystems Inc., Foster City, CA, where he managed a group of ten engineers and scientists (six Ph.D. doctors). Previously, in a singular capacity as the only Microfluidics Engineer, he developed commercial product called InkWells™ from concept to a commercial product at Nano Ink, Inc. Inkwells are microfluidic platforms used for bio/nanotechnology applications. He has one issued patent, submitted four provisional patent applications, five patents pending, and more than 20 invention disclosures while working at ABI, CIPHERGEN Biosystems, Nano Ink, and Coventor, Inc. His research interests are in thermofluidics (boiling), MEMS/microfluidics, and nanotechnology.

Dr. Banerjee received the "2001 Best Journal Paper Award" from the ASME Heat Transfer Division (HTD). He was invited to the membership of four national academic honor societies. At the graduation convocation at IIT he received the "Amlan Sen Best Mechanical Engineering Student Award (Endowment)." He also received the "Jagdish Bose National Science Talent Scholar" award from the Government of India. He received the "New Investigator Award (2005)" from the Texas Space Grants Consortium (TSGC), the "ASEE Summer Faculty Fellowship (2006, 2007)" at the Air Force Research Labs (AFRL), and "Morris Foster Fellowship (2007–2008)" from the Mechanical Engineering Department at Texas A&M University.